

# Detailed investigation of capillary active insulation materials by $^1\text{H}$ nuclear magnetic resonance (NMR) and thermogravimetric drying

Sarah M. MUNSCH<sup>1\*</sup>, Thilo BINTZ<sup>1</sup>, Rüdiger HEYN<sup>2</sup>, Hauke HIRSCH<sup>2</sup>, John  
GRUNEWALD<sup>2</sup>, Sabine KRUSCHWITZ<sup>1,3</sup>

<sup>1</sup> Department of Non-destructive Testing, Bundesanstalt für Materialforschung und -prüfung; Berlin, Germany

<sup>2</sup> Institute of Building Climatology, Technical Universität Dresden; Dresden, Germany

<sup>3</sup> Institute for Civil Engineering, Technical Universität Berlin; Berlin, Germany

\*Corresponding author, e-mail address: [sarah.munsch@bam.de]

## Abstract

Capillary active interior insulation materials are an important approach to minimize energy losses of historical buildings. A key factor for their performance is a high liquid conductivity, which enables redistribution of liquid moisture within the material. We set up an experiment to investigate the development of moisture profiles within two different interior insulation materials, calcium-silicate (CaSi) and expanded perlite (EP), under constant boundary conditions. The moisture profiles were determined by two different methods: simple destructive sample slicing with subsequent thermogravimetric drying as well as non-destructive NMR measurements with high spatial resolution. The moisture profiles obtained from both methods show good agreement, when compared at the low spatial resolution of sample slicing, which demonstrates the reliability of this method. Moreover, the measured  $T_2$ -relaxation-time distributions across the sample depth were measured, which may give further insight into the saturation degree of the different pore sizes. In order to explain differences in the moisture profiles between CaSi and EP, we determined their pore-size distribution with different methods: conversion of the NMR  $T_2$  relaxation-time distribution at full saturation, mercury intrusion porosimetry and indirect determination from pressure plate measurements. CaSi shows a unimodal distribution at small pore diameters, while in EP, a bi-modal or wider distribution was found. We assume that the smaller pore diameters of CaSi lead to a higher capillary conductivity, which causes a more distributed moisture profile in comparison with that of EP.

**Keywords:** insulation materials; nuclear magnetic resonance; capillary conductivity; pore-size distribution

## 1 Introduction

Interior insulation materials are an important component for energetic retrofitting of historic and heritage buildings. When a historic façade needs to be preserved, the use of insulation materials is the only available technology to lower the thermal transmissions of the building walls. It is often also an important precondition for the transition from fossil-based to renewable heating systems, such as heat pumps.

Interior insulations, in principle, can create moisture damages inside the wall, as vapor from the warm humid room may condensate between the wall and the interior insulation. Modern materials for interior insulation therefore rely on the capillary redistribution of the condensate. In particular, they have a high capillary conductivity, which causes transport of liquid moisture in opposite direction to the vapor transport, i. e. a redistribution from the exterior wall to the room. This phenomenon is described in detail by [1] and is often called “capillary-active”.

As described in WTA sheet 6.2 [2], modern software for hygrothermal simulations is capable of modeling both transport mechanisms, allowing to assess constructions with interior insulations and prevent damages due to excessive interstitial condensation. However, to reach reliable simulation results, the hygrothermal properties, especially the transport coefficients need to be determined based on carefully designed non-isothermal experiments. Conventional experiments like the water-uptake-experiment or the drying-experiment may not be



sufficient [3]. Therefore, we set up an experiment that replicates typical interior insulation conditions. A material sample is subjected to a warm humid climate on one side and a low temperature on the other side. Vapor transport occurs towards the cold side, while capillary transport takes place in the opposite direction, causing some redistribution of the moisture. We measure the resulting moisture profile in the samples between both sides using two different methods: simple sample slicing and Darr-drying as well as sophisticated NMR measurements with high spatial resolution. NMR allows us to validate the method of simple sample slicing. Moreover, it gives deeper insights into the moisture storage behavior and the pore space of the studied material, which is also important for hygrothermal simulations.

## 2 Theory of nuclear magnetic resonance

$^1\text{H}$  nuclear magnetic resonance (NMR) measures the interaction of  $^1\text{H}$  protons with a static magnetic field. When a sample containing hydrogen protons is placed within a static magnetic field  $B_0$ , due to their spins, the protons act like bar magnets and align with  $B_0$ . Thereby, a magnetization parallel to  $B_0$  builds up that precesses with the so-called Larmor frequency  $f_0$ . By applying a radiofrequency pulse  $B_1$  perpendicular to  $B_0$  having the same frequency as  $f_0$ , leads to the desired resonance effect and the magnetization is tipped by  $90^\circ$  from the longitudinal axis into the transverse plane. After the pulse, the protons and therefore the magnetization precess back into the equilibrium state and align with  $B_0$  again. Consequently, an exponentially decaying signal ( $T_2$  relaxation) can be measured within the transverse plane (equation (1)). In fact, within a porous media containing various pore sizes, the measured signal is a sum of numerous decaying signals having different  $T_2$  times as exponents.

$$M_{xy}(t) = M_{0,xy} e^{-\frac{t}{T_2}} \quad (1)$$

with  $t$  as the time;  $T_2$  as the transverse relaxation time;  $M_{xy}$  as the magnetization in the transverse plane and  $M_{0,xy}$  as the magnetization at  $t = 0$ .

The measured  $T_2$  NMR signal depends on the protons' amount and mobility within the sample. The mobility is thereby influenced by the pore sizes as well as their physical and chemical bonding. Therefore, properties that may be determined are the moisture content, the porosity and the pore-size distribution. To obtain the moisture content or the porosity, only the maximum amplitude of the decaying signal is needed. However, to obtain information on the protons' mobility and the pore sizes, the measured signal has to be numerically inverted based on multi-exponential fitting. In this way, a distribution of the relaxation times can be calculated.

At full saturation, the obtained distribution can be converted into a pore-size distribution, as the relaxation time is directly proportional to the water-covered-surface-to-water-filled-volume ratio of the pores [4]. Moreover, a material constant, the surface relaxivity  $\rho$  in  $\mu\text{m/s}$ , has to be known or determined. Using equation (2), then, the time axis of the relaxation-time distributions can be converted into a pore size axis. Regarding equation (2), there are two ways to determine  $\rho$ : 1. if  $S_{Pore}/V_{Pore}$  is known, it can be directly calculated; 2. the NMR curve can be compared to the pore-volume distribution of a comparison method such as mercury intrusion porosimetry (MIP). Under assumption of a pore geometry (e. g. cylindrical means  $c=2$ ),  $\rho$  can be manually adopted until the curves lay congruent one above the other.

$$\frac{1}{T_2} = \frac{S_{Pore}}{V_{Pore}} \rho = \frac{c}{r} \rho \quad (2)$$

with  $S_{Pore}$  as the water-covered pore surface;  $V_{Pore}$  as the water-filled pore volume;  $\rho$  as the surface relaxivity;  $c$  as the geometry factor and  $r$  as the pore radius.

Further details on the general principle of NMR and its evaluation as well as various application fields may be found in [5], [6] and [7].

### 3 Condensation test

#### 3.1 Materials and sample preparation

We investigated two different materials, calcium-silicate (CaSi) and expanded perlite (EP), which are both widely applied as interior insulation for buildings and show a comparable thermal conductivity (see **Table 1**). Both have a high porosity and a relatively low vapour resistance-factor  $\mu$ , which describes the vapour diffusivity in relation to that of air. However, CaSi has a significantly lower  $\mu$  than EP, i. e. a higher vapour diffusivity. Reasons for the different transport parameters are most likely due to the different production processes. CaSi is produced by use of a foaming agent in large blocks. So, a widely connected network of capillaries is formed. The investigated EP-boards are produced from expanded Perlite pellets, that are chemically or physically bound into boards. The porosity of these pellets is reached by heating the natural raw material, perlite, a volcanic glass, to high temperatures, so that inside trapped water vaporizes and expands the material. The expanding into pellets and subsequent bounding may result in less widely connected networks of capillaries with various pore sizes. For both materials, we prepared samples of 100 mm x 100 mm x 50 mm. One surface of 100 mm x 100 mm was left unchanged, while all other lateral sides were sealed with paraffin, in order to make them vapour- and watertight. The samples were glued on an aluminium sample carrier of 10 mm thickness and all lateral coated sides were also insulated with an EPDM insulation.

**Table 1:** Material properties.

	Thermal conductivity [W/(mK)]	Density [kg/m <sup>3</sup> ]	Vapour resistance factor $\mu$ [-]	Effective porosity [Vol.-%]
CaSi	0.059	186.9	2.7	93
EP	0.055	151.8	7.7	88

#### 3.2 Experimental set-up

The set-up is depicted in **Figure 1** and described by Hirsch et.al. [3]. It emulates a typical interior insulation scenario, where the material is exposed to a warm humid climate (the room) on one side and a cold temperature (the building wall) on the other side. Therefore, we expose the unchanged side of the samples to a climate chamber with 23 °C and a relative humidity of 70 %. The opposite sealed side with the sample carrier is cooled by an aluminium cooling plate, connected to a laboratory chiller and controlled to a temperature of 5 °C.

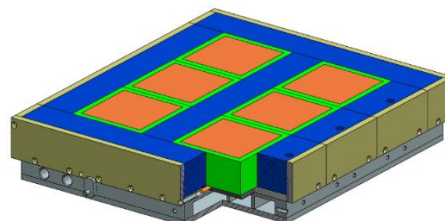


**Figure 1:** Experimental set-up with samples (orange), EPDM insulation (green), XPS insulation (blue) and cooling plate (grey).

The set-up comprises 3 samples (no. 4, 5 and 6) of each material, which are placed next to each other and insulated against the climate chamber with XPS, to obtain a nearly one-dimensional temperature distribution.

### **3.3 Measurement procedure**

We kept the set-up under constant boundary conditions over a period of 55 days. Every 3 to 4 days, we disassembled the set-up and weighted the samples. After finishing the experiment, we measured the moisture content profile in vertical direction, i. e. from the warm and exposed side to the cooled and sealed side. Therefore, we applied two different methods: Sample slicing and NMR measurements. For sample slicing, sample no. 5 was immediately cut into five horizontal slices of about 10 mm thickness. We determined the moisture content by thermogravimetric drying using a drying temperature of 45 °C [8].

### **3.4 NMR measurement settings**

The NMR measurements were conducted with the NMR tomograph that uses a permanent magnet with a field strength of 0.21 T (8.9 MHz). With the maximum measurable sample diameter of 72 mm, the samples no. 4 and 6 of both materials had too large dimensions to be directly measured. Therefore, they were divided in 4 equal pieces. This resulted in 4 cuboids (A, B, C, D) with edge lengths of around 50 mm. With a resulting diagonal length of around 70 mm, still the largest available coil with the max. sample diameter of 72 mm had to be used. To avoid any drying of the cut surfaces during the measurements, the samples were wrapped in foil.

We measured high resolved moisture profiles along the whole sample height by applying slice-selective measurements with a slice thickness of 2 mm. Starting at the bottom of a sample, this resulted in a total of 26 slices per sample. For the  $T_2$  measurement, we used the Carr-Purcell-Meiboom-Gill pulse sequence with a minimum echo time of 80  $\mu$ s. The  $T_2$  signal was recorded for 300 ms in all samples. To obtain an adequate signal-to-noise ratio, one single measurement consisted of 16 to 24 stacks. The measured amplitude was then converted into a volumetric moisture content using a water sample measurement as reference.

## **4 Determination of the pore-size distribution**

We determined the pore-size distribution of both materials with three different methods: NMR, pressure plate measurements (PP) and MIP.

### **4.1 NMR at full saturation**

Besides the measurement of moisture profiles during the condensation test, a sister sample from both EP and CaSi was also measured at full saturation state for comparison and for the determination of the pore-size distribution. To obtain full saturation, the samples were first dried at 40 °C, then evacuated with 7 mBar using a vacuum pump and subsequently flooded with tap water. In contrast to the partially saturated samples, we only measured one slice in the middle of the sample height in the fully saturated samples. Moreover, the signal had to be recorded for a longer time as relaxation in full saturated pores is slower. Therefore, the  $T_2$  signal of the EP sample was recorded for 8 s and the signal of the CaSi sample for 2.5 s instead of 300 ms. As described above, the fully saturated samples were also wrapped in foil during the measurement and the amount of signal stacking remained the same.

The signal of the fully saturated samples as well as the complete profile of the samples EP4\_D and CaSi6\_D were then numerically inverted by use of the software NUCLEUSinv provided by Thomas Hiller (<https://github.com/ThoHiller/nmr-nucleus>) to obtain the  $T_2$  relaxation-time distributions.

#### **4.2 Pressure plate measurement**

Applying the PP method [9], saturated samples are exposed to different pressures stages and their moisture content is determined after each stage through drying and weighing. After saturating the samples by underwater submersion, we put them in small pressure chambers and subsequently exposed them to pressures from 30 hPa to 8000 hPa. Thereby, the samples are placed on a fully saturated ceramic plate, in order to allow water to easily escape the sample.

#### **4.3 Mercury intrusion porosimetry**

The mercury intrusion porosimetry (MIP) measurements [10] were conducted with the AutoPore V from Micromeritics (Norcross, USA). Using this device, mercury can be intruded with a pressure ranging from 4 kPa to 400 MPa. This first results in a cumulative intruded mercury volume versus pressure curve, which then can be converted into a pore-throat distribution. The conversion is done by applying the Washburn equation under assumption of cylindrical pore throat shapes.

### **5 Results and discussion**

#### **5.1 Moisture profile measurements**

**Figure 2** shows the moisture profiles measured with NMR for both EP and CaSi after 55 days in the condensation experiment, described in section 3. When the condensation experiment was stopped, the EP samples were still showing continued moisture gain. This was not the case for the CaSi samples. The top position (0 mm) represents the warm humid side and the bottom position (50 mm) the cold sealed side of the sample. As described above, the measured amplitudes are converted into volumetric moisture contents. The determined moisture contents range from 0 Vol.-% up to around 15 Vol.-%. As expected, moisture mainly gathers at the lower cold side. In general, it can be noticed that all 8 sister samples of one material show a similar moisture ingress.

Comparing the moisture ingress in the EP and CaSi samples, the CaSi samples show a higher moisture ingress. While the moisture content is around 0 Vol.-% in the upper 15 mm in the EP samples, in the CaSi samples the moisture content steadily increases over the whole sample depth until 35 mm depth. Then it reaches a constant value of 11 Vol.% to 12 Vol.-%. Only the last value on the bottom of the sample has a higher value. In contrast, in the EP samples, the moisture content starts to increase at 15 mm sample depth and then reaches a constant value also at 35 mm sample depth, but having a steeper gradient compared to the CaSi samples.

We assume the significant difference in the profiles of EP and CaSi to be caused by differences in their vapor diffusivities as well as the capillary conductivities, which may result from different pore sizes. CaSi has a higher capillary conductivity and therefore more moisture is redistributed towards the upper (warm and humid) sample surface. In summary, this results in the same moisture content on the humid side, but in differences regarding the total moisture content. In total, the EP samples reached moisture contents of 6.3 Vol.-% to 6.7 Vol.-% (see

legend in **Figure 2**), while the CaSi samples contain a total moisture content of around 7.5 Vol.-% to 8.3 Vol.-%.

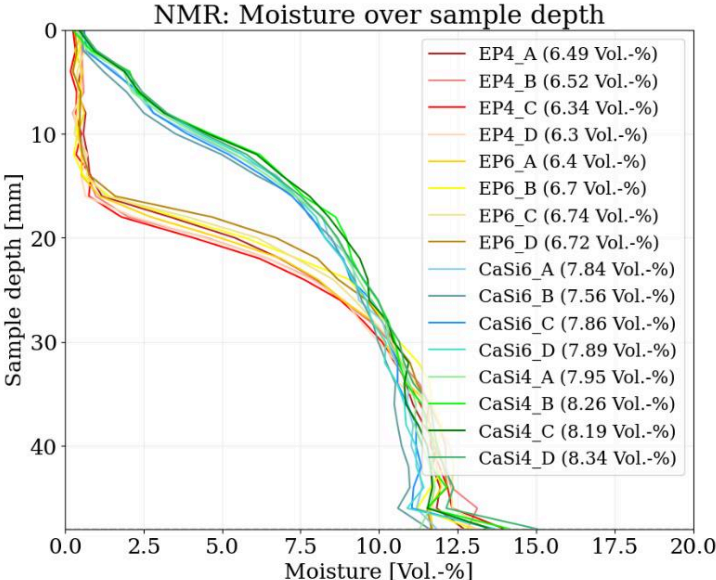


**Figure 2:** Moisture profile over sample depth determined with <sup>1</sup>H NMR in EP and CaSi samples; in the legend the total moisture content of the samples determined with NMR is given.

The moisture profiles obtained with NMR were then compared to the moisture profile of sister sample no. 5, which was first cut into 5 slices and then oven dried. As the NMR moisture profile has a higher spatial resolution, the NMR profile was reduced to 5 data points by forming the mean value of 5 adjacent 2 mm slices. The results are shown in **Figure 3**.

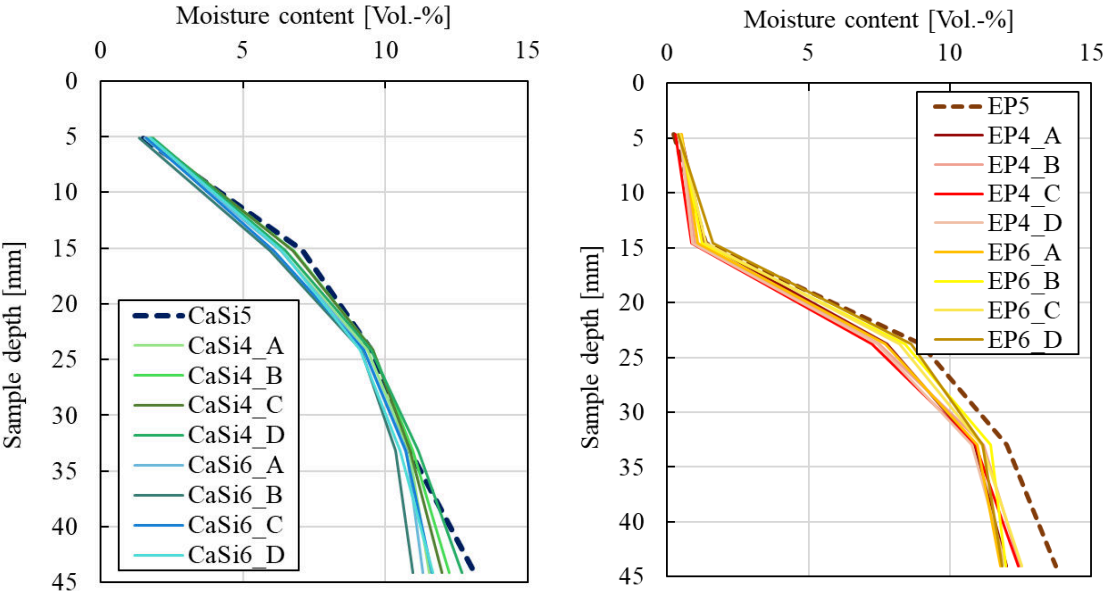


**Figure 3:** Comparison of moisture profiles over sample depth determined with NMR (sample 4 and 6) and Darr drying after slicing (sample 5); left: CaSi samples; right: EP samples.

The moisture profiles determined with sample slicing (dashed lines) match those from NMR measurements relatively well. As it could be seen in the NMR results in **Figure 2**, in contrast to CaSi5, EP5 only has a low moisture content (< 0.5 Vol.%) in the upper 15 mm, but a steeper moisture gradient from 15 mm to 35 mm sample depth. However, in comparison to the sister samples measured with NMR, EP5 has a slightly higher moisture content in the lower half of the sample. Regarding the CaSi samples, the moisture content of CaSi5 is only minimally higher on the bottom of the sample.

In fact, we generally expected a lower of moisture content in the samples EP5 and CaSi5 as the slicing may cause a heat input and an increase of surfaces, over which the samples may dry out more rapidly. However, this phenomenon could not be observed. In contrast, the sister samples measured with NMR contained a slightly lower moisture content, especially in the bottom sample half. Indeed, the NMR samples also had to be cut in four pieces to be measured, which may have caused a minimal loss of moisture. Although, they were wrapped in foil immediately, a loss of moisture cannot be excluded.

## 5.2 $T_2$ relaxation-time distributions over sample height

The NMR measurements over sample depth of the two samples CaSi6 and EP4 were also numerically inverted to obtain  $T_2$  relaxation-time distributions. As explained above, this gives information on the hydrogen proton mobility and the pore sizes. For comparison, we also measured a 2 mm slice from the middle of a fully saturated sister sample, which represents a pore-size distribution. Indeed, the distribution has to be converted by use of a material constant that can be determined by comparisons with further pore-size distribution measurements. This is shown in 5.3.

The resulting  $T_2$  relaxation-time distributions are presented in **Fehler! Verweisquelle konnte nicht gefunden werden.** Regarding the full saturation distribution (black dashed line), the CaSi material has a unimodal distribution and the EP material a bimodal distribution. In CaSi6, the main relaxation time lays at around 80 ms at full saturation and shifts from 7 ms to 1 ms from sample bottom to sample top during the condensation test. In EP4, the two relaxation time peaks lay at 1s and 0.2 s. In the condensation test, the main  $T_2$  relaxation time shifts from 0.1 s to around 2 ms and the second peak shifts from around 1 ms to 0.2 ms.

The shift of relaxation time results from the reduced proton mobility caused by two main reasons: 1. the moisture gathers in smaller pores, where the protons are spatially limited; 2. the pores are only partially saturated, which means that the hydrogen protons are strongly bound to the pore wall and therefore significantly restricted in their mobility.

As CaSi seems to contain one dominant pore size (unimodal distribution at full saturation) and as the distributions measured during the condensation lay outside the full saturation curve, the shift may only result from partial saturation of the main existing pore size. For the EP material it becomes more complicated as it contains a larger range of pore sizes. It is visible in the range of 0.1 s and 1 s that fractions of the distributions measured during the condensation test lay in the range of the full saturation curve. Consequently, a fraction of pores may already be fully saturated. However, in the range of short relaxation times at around 0.2 ms and 1 ms, a clear distinction between the saturation degree of the two existing pore sizes is not possible.

Nevertheless, the completely different developments of the measured distributions may explain the differences observed in the moisture profiles over sample depth. CaSi only has one dominant  $T_2$  relaxation time (i. e. pore size), that is smaller than in EP. As we obtained an identical surface relaxivity for both materials (following subsection), it follows that CaSi contains significantly smaller pores than EP. These smaller pore sizes cause a higher capillary

conductivity and therefore a more uniform distribution of the moisture profile is observed in CaSi, which is in contrast to the sharper gradient found in EP. Due to the smaller pores and stronger capillary conductivity in CaSi, more moisture is transported to the upper (drier) part of the material.

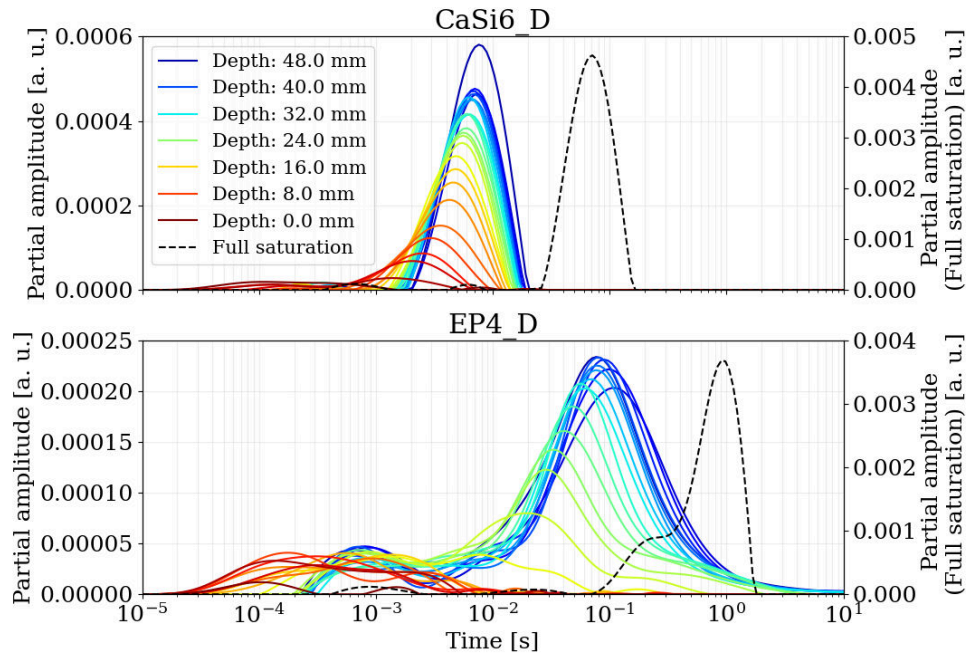


**Figure 4:**  $T_2$  relaxation-time distributions measured at different depths of the samples CaSi6\_D (top) and EP4\_D (bottom) measured during the condensation test; the distribution at full saturation was measured within a sister sample.

### 5.3 Determination of the pore-size distribution

$T_2$  relaxation-time distributions measured in a fully saturated sample also represent a pore-size distribution. Therefore, the NMR full saturation measurements from **Figure 4** were compared to pore-size distributions obtained with MIP and PP measurements. The information about the pore sizes may also confirm the observations and explanations from above. The effective porosity determined with each method thereby also gives information about how much connected pore space could be resolved. The porosity values and the dominant pore sizes determined with all three methods are summarized in **Table 2**.

The resulting pore-size distributions obtained with MIP, PP and NMR are shown in **Figure 5**. The surface relaxivity, which is needed to convert the NMR relaxation-time distributions into pore size distributions, was determined by the comparison with the MIP results and finally set to  $2.5 \mu\text{m/s}$  for both EP and CaSi. For both methods a cylindrical pore geometry was assumed. Comparing the distributions for the CaSi material, all three methods resulted in an almost unimodal distribution. The dominant pore-size lays at around  $0.3 \mu\text{m}$  (PP) and  $0.7 \mu\text{m}$  (NMR and MIP). In fact, the pore size obtained with the PP lays slightly under the value obtained with NMR and MIP. However, there is a dependence between NMR and MIP as the latter was used as reference for NMR. The effective porosity of CaSi lays at around 90 Vol.-% to 95 Vol.-%, whereby NMR measured the highest effective porosity.



**Table 2:** Porosities and dominant pore sizes of CaSi and EP determined with MIP, NMR and PP.

	CaSi		EP	
	Effective porosity [Vol.-%]	Dominant pore size [ $\mu\text{m}$ ]	Effective porosity [Vol.-%]	Dominant pore size [ $\mu\text{m}$ ]
NMR	95	0.7	85	2.8/ 18
MIP	90	0.7	88	2.8/ 18
PP	93	0.3	88	65

For the EP material, with all three methods, a wider distribution was determined. While with MIP and NMR bimodal distributions with high amplitudes at 2.8  $\mu\text{m}$  and 18  $\mu\text{m}$  could be observed, with the PP method a somewhat wider, but unimodal distribution with a maximum at around 65  $\mu\text{m}$  was observed. However, in contrast to NMR, MIP also measured pore volume within this range. The effective porosity in EP is slightly lower than in CaSi reaching values from 85 Vol.-% (NMR) to 88 Vol.-% (MIP, PP).

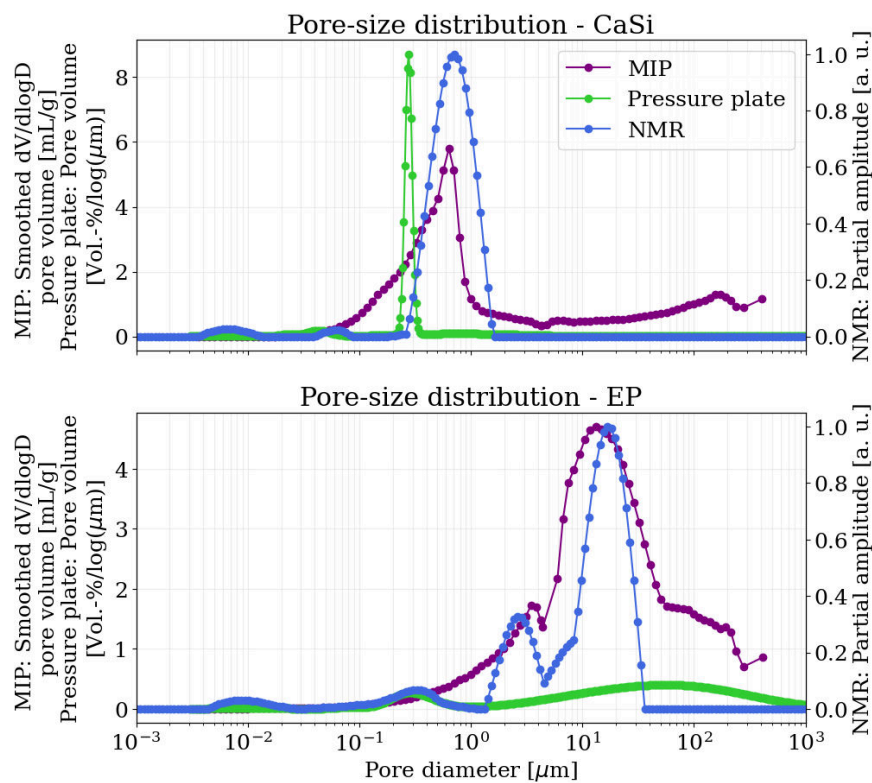


**Figure 5:** Comparison of pore-size distributions obtained with MIP, PP measurements and NMR (surface relaxivity = 2.5  $\mu\text{m/s}$ ); top: CaSi samples; bottom: EP samples.

Regarding the NMR curves for both materials, two further small peaks below 1  $\mu\text{m}$  could be observed. The first lays at around 0.007/ 0.008  $\mu\text{m}$  and was not measured with MIP and the PP measurement. In fact, this could be chemically or physically bonded water or even an artefact of the numerical inversion. The second peak lays at 0.07  $\mu\text{m}$  for CaSi and 0.4  $\mu\text{m}$  for EP. For both materials, this peak was also resolved with the PP measurement and covered from the MIP distribution.

Although the methods are based on completely different principles and measurands, with all three methods similar distributions could be obtained. The major discrepancies, however, lay in the location of the dominant pore size obtained with PP. While the NMR relaxation time at full saturation is proportional to the water-covered surface to water-filled volume ratio of the pores, both MIP and PP directly measure the pressure needed to intrude mercury or extrude water. Nevertheless, MIP is mainly based on adsorption of a non-wetting fluid, but PP on the desorption of water. Therefore, effects such as the ink-bottle effect cannot be excluded and may be the cause for the observed differences.

Another aspect that has to be mentioned is the fact, that MIP and PP are more sensitive to pore throats and NMR more to pore bodies [11]. However, when a capillary bundle pore model is assumed, the NMR relaxation is thought to be more strongly influenced by the diameter than the length of cylindrical pores. Therefore, the distributions may be directly comparable.

## 6 Conclusion

Newly developed “capillary-active” insulation materials show two forms of moisture transport that occur in opposite directions. To be able to assess constructions with interior insulations and prevent damages due to excessive interstitial condensation, trustworthy simulations of their hygrothermal behavior are increasingly in demand. As input for simulation, the transport coefficients are used, which are obtained from measured moisture ingress profiles.

Therefore, in this work, low-resolution and destructively measured moisture ingress profiles obtained from slicing and drying were compared to profiles measured non-destructively and with high resolution by use of NMR. For the two materials tested here, CaSi and EP, both methods resulted in congruent results. Although NMR is a non-destructive method, the samples had to be cut to fit into the tomograph. In fact, this may also have led to an undesired moisture loss.

However, the authors conclude, that, if possible, the use of NMR (with the right sample size) represents the better choice as it delivers high resolution profiles. Moreover, it also gives information regarding the pore-size and consequently the moisture distribution within the pore space. In detail, the additionally analysed  $T_2$  relaxation-time distributions enabled an explanation for the different moisture ingress behaviour that could be observed in EP and CaSi. The final conversion into pore-size distributions, proofed that the main cause lays in the pore sizes and consequently in the different capillary conductivities and vapor diffusivities. In CaSi, which contains smaller pores than EP, therefore a stronger moisture redistribution (stronger moisture ingress but also return transport) occurred. This resulted in the same moisture content on the humid side for both CaSi and EP, but in a higher moisture content on the warm side as well as in total for CaSi.

Moreover, the results also showed that NMR seems to be suitable for the determination of pore-size distributions in materials such as calcium-silicate and expanded perlite. As the for the conversion needed surface relaxivity was unknown for both materials, it was determined by comparison with MIP and resulted in a value of  $2.5 \mu\text{m/s}$  for both. Finally, after the conversion, all dominant pore sizes that were determined with MIP and PP measurement could also be resolved with NMR. The effective porosities obtained with all three methods also laid close together with a maximum deviation of 5 Vol.-% for CaSi and 3 Vol.-%.

## Acknowledgements

The authors are grateful to Carsten Prinz and Annett Zimathies for conducting the mercury intrusion porosimetry measurements. Moreover, the authors thankfully acknowledge the founding by the German Ministry of Economic Affairs and Climate Action (BMWK) for the research project “NaVe” under the project number 03ET1649A.

## References

- [1] A. Binder, D. Zirkelbach and H. Künzel, “Test method to quantify the wicking properties of porous insulation materials designed to prevent interstitial condensation,” in *AIP Conference Proceedings*, American Institute of Physics, 2010, pp. 242-247.
- [2] WTA, “6.2 Leaflet - Simulation of heat and moisture transfer,” WTA Publications, Vol. 30, München, Germany, 2014.
- [3] H. Hirsch, R. Heyn and P. Klößeiko, “Capillary condensation experiment for inverse modelling of porous building materials,” *E3S Web of conferences*, EDP Sciences, p. 17003, 2020.
- [4] K. R. Brownstein and C. E. Tarr, “Importance of classical diffusion in NMR studies of water in biological cells,” *The American Physical Society*, vol. 19, pp. 2446-2453, 1979.
- [5] G. R. Coates, L. Xiao and M. Prammer, *NMR Logging - Principles & Applications*, Houston: Halliburton Energy Services, 1999.
- [6] K.-J. Dunn, D. J. Bergman and G. A. Latorraca, *Nuclear magnetic resonance - Petrophysical and logging applications*, Handbook of Geophysical Exploration, Elsevier, 2002.
- [7] S. M. Nagel, C. Strangfeld and S. Kruschwitz, “Application of 1H proton NMR relaxometry to building materials –A review,” *Journal of Magnetic Resonance Open* 6-7, 2021.
- [8] DIN EN ISO 12570, “Hygrothermal performance of building materials and products — Determination of moisture content by drying at elevated temperature (ISO 12570 : 2000); German version,” DIN Deutsches Institut für Normung e.V., Berlin, 2000-04.
- [9] ISO 11274, “Soil quality - Determination of the water-retention characteristic - Laboratory methods,” ISO, Geneva, Switzerland, 2019.
- [10] ISO 15901-1, “Evaluation of pore size distribution and porosimetry of solid materials by mercury porosimetry and gas adsorption — Part1: Mercury porosimetry,” ISO, Geneva, Switzerland, 2005.
- [11] S. Kruschwitz, M. Halisch, R. Dlugosch and C. Prinz, “Toward a better understanding of low-frequency electrical relaxation — An enhanced pore space characterization,” *GEOPHYSICS, VOL. 85, NO. 4*, pp. MR257-MR270, 2020.